

# Mg<sub>2</sub>Si<sub>x</sub>Sn<sub>1-x</sub> heterostructures on Si(111) substrate for optoelectronics and thermoelectronics

Nikolay G. Galkin<sup>\*a</sup>, Konstantin N. Galkin<sup>a</sup>, Sergey A. Dotsenko<sup>a</sup>, Igor M. Chernev<sup>a</sup>, Andrei M. Maslov<sup>a</sup>, L. Dózsa<sup>b</sup>, B. Pécz<sup>b</sup>, Z. Osváth<sup>b</sup>, I. Cora<sup>b</sup>, D.B. Migas<sup>c</sup>, R. Kudrawiec<sup>d</sup> and J. Misiewicz<sup>d</sup>  
<sup>a</sup>Institute of Automation and Control Processes Far Eastern Branch of Russian Academy of Sciences, 5, Radio Street, 690041, Vladivostok, Russia

<sup>b</sup>Institute of Technical Physics and Materials Research, Centre for Energy Research, Hungarian Academy of Sciences, 1525 Budapest Pf. 49, Hungary

<sup>c</sup>Belarusian State University of Informatics and Radioelectronics, P. Brovka, 6, 220013 Minsk, Belarus

<sup>d</sup>Wrocław University of Technology, Wrocław, 50-370, Poland

## ABSTRACT

Thin (50-90 nm) non-doped and doped (by Al atoms) Mg<sub>2</sub>Sn<sub>0.6</sub>Si<sub>0.4</sub> and Mg<sub>2</sub>Sn<sub>0.4</sub>Si<sub>0.6</sub> films with roughness of 1.9-3.7 nm have been grown by multiple deposition and single annealing at 150 °C of multilayers formed by repetition deposition of three-layers (Si-Sn-Mg) on Si(111) p-type wafers with 45 Ω·cm resistivity. Transmission electron microscopy has shown that the first forming layer is an epitaxial layer of hex-Mg<sub>2</sub>Sn(300) on Si(111) substrate with thickness not more than 5-7 nm. Epitaxial relationships: hex-Mg<sub>2</sub>Sn(300)|| Si(111), hex-Mg<sub>2</sub>Sn[001]|| Si[-112] and hex-Mg<sub>2</sub>Sn[030]|| Si[110] have been found for the epitaxial layer. But inclusions of cub-Mg<sub>2</sub>Si were also observed inside hex-Mg<sub>2</sub>Sn layer. It was found that the remaining part of the film thickness is in amorphous state and has a layered distribution of major elements: Mg, Sn and Mg without exact chemical composition. It was established by optical spectroscopy data that both type films are semiconductor with undispersed region lower 0.18 eV with  $n_0 = 3.59 \pm 0.01$ , but only two direct interband transitions with energies 0.75-0.76 eV and 1.2 eV have been determined. The last interband transition has been confirmed by photoreflectance data at room temperature. Fourier transmittance spectroscopy and Raman spectroscopy data have established the formation of stannide, silicide and ternary compositions.

**Keywords:** Mg stannide, silicide, structure, optical properties, band structure

## 1. INTRODUCTION

Magnesium-silicides-stannides ternary alloys (Mg<sub>2</sub>Si<sub>x</sub>Sn<sub>1-x</sub>)<sup>1-2</sup> are well known as eco-friendly semiconductor materials. These alloys<sup>3</sup> possess a large Seebeck coefficient, high electrical conductivity, low thermal conductivity and high value of power factor that are perspective for creation of efficient thermoelectric converters and interesting for individual optoelectronics tasks as low band gap semiconductor.

The Mg<sub>2</sub>Si<sub>1-x</sub>Sn<sub>x</sub> ternary alloy is a perspective material also from the point of view of their increasing conductivity due to their smaller band gap than that of its components and decrease of its thermal conductivity due to complex phonon structure of the ternary alloy<sup>4,5</sup>. The detailed research of Mg<sub>2</sub>X (X=Si, Sn, Ge) compounds and their quasi-binary alloys<sup>2</sup> have shown that Mg<sub>2</sub>Si - Mg<sub>2</sub>Sn system is preferable for thermoelectrical applications due to a combination of electrical properties and peculiarities of the band structure. Since Si and Sn have the large difference in atom masses, the Mg<sub>2</sub>Si<sub>1-x</sub>Sn<sub>x</sub> solid alloys possess the lowest lattice thermal conductivity in the above group.

\*galkin@iacp.dvo.ru; phone +7 423 2310-687; fax +7423 2310-452

The problem of doping of  $Mg_2X$  compound and their ternary alloys is the main problem for them as thermoelectric materials. It is known that the compound non-stoichiometric influences on the conductivity type of these compounds.  $Mg_2Si$  monocrystals grown from stoichiometric Mg/Si melt composition without additional doping have n-type conductivity <sup>6</sup>, while  $Mg_2Ge$  monocrystals grown from stoichiometric melt are p-type conductivity semiconductor <sup>7</sup>. However for  $Mg_2Si$ ,  $Mg_2Sn$  and  $Mg_2Si_xSn_{1-x}$  ternary alloy this effect is not exactly determined. It is also known that Ag, Ga and Cu atoms act as donor impurities for  $Mg_2X$  ( $X=Si, Sn, Ge$ ) compounds <sup>8,9</sup>. Recently it was found that in the non-doped  $Mg_2Sn$  polycrystalline films grown by solid phase epitaxy from Sn-Mg multilayers on Si (111) n-type substrate has a complex conductivity and carrier mobility behavior, which is explained by change of hole conductivity at low temperature (100-230 K) on the electron conductivity at temperatures 250-420 K due to beginning of intrinsic conductivity in  $Mg_2Sn$  film <sup>10</sup>. However  $Mg_2Si_xSn_{1-x}$  ternary alloy films have not been grown on atomically clean Si(111) surface and have not been studied their structure and optical properties.

In this work the solid phase growth of undoped and Al doped  $Mg_2Sn_xSi_{1-x}$  alloy semiconductor on atomically clean boron doped (p-type) silicon substrate (Si(111)7x7) was tested, the structural and optical properties of the grown films were studied by transmission electron microscopy, Raman spectroscopy, optical spectroscopy, photoreflectance spectroscopy and analyzed.

## 2. EXPERIMENT

Growth experiments were carried out in ultra-high vacuum (UHV) chamber: VARIAN with base pressure of  $2 \cdot 10^{-9}$  Torr equipped with AES-EELS spectrometer, sublimation sources of Si, Sn and Mg and quartz sensors of film thickness. Si(111) p-type wafers with 45  $\Omega \cdot cm$  resistivity were used as substrates for growth experiments. The silicon cleaning procedure and growth processes were explained in <sup>10</sup>. The solid phase epitaxy (SPE) method of  $Mg_2Sn_xSi_{1-x}$  growth was used in our experiments with annealing temperature of 150 °C. During the thin  $Mg_2Sn_xSi_{1-x}$  film the formation of amorphous silicon layer (a-Si) was a first one on Si(111)7x7 and then the Sn and Mg atoms were deposited at room temperature. Deposition of a-Si, Sn and Mg was repeated at room temperature 8 times. For variation of  $Mg_2Sn_xSi_{1-x}$  film composition different thicknesses of Sn and Mg and the same Si thickness were deposited. Calculated compositions were the next:  $Mg_2Sn_{0.4}Si_{0.6}$  and  $Mg_2Sn_{0.6}Si_{0.4}$ . After that an annealing at 150 °C was performed. The doping of one grown film was performed account for the deposition of small portion of Al atoms between Sn and Mg in each three-layer Si-Sn-Mg with following annealing at 150 °C of all grown Si-Sn-Mg system. The Sn, Mg, Si and Al deposition rates (0.3 – 1.5 nm/min) were controlled by quartz microbalance system.

The morphology of grown samples was investigated *ex situ* by atomic force microscopy (AFM) in contact and tapping modes. The optical reflectance spectra of grown systems were registered on automatic spectrophotometer Hitachi U-3010 in the energy range of 0.1-6.2 eV (with integrated sphere at 1.5 – 6.2 eV) and on Furies-spectrophotometer BRUKER Vertex 80v in the infrared wavelength (1 – 100  $\mu m$ ). Raman spectra were registered at room temperature on "WITec alpha 300 RSA+" confocal Raman microscope (ITP&MS HAS, Hungary) with exiting wavelength of laser of 488 nm. A Philips CM 20 TEM at 200 keV was used to measure cross-sectional specimens, and a JEOL 3010 HR TEM equipped with an energy filtering attachment (EFTEM) was also applied. Photoreflectance spectra were measured at room temperature with monochromator HORIBA JobinYvon, light source, laser beam, lock-in amplifier and modulator (Poland).

## 3. RESULTS AND DISCUSSIONS

After UHV growth and re-loading from vacuum chamber the morphology of three samples was studied by AFM. The first sample has proposed composition  $Mg_2Sn_{0.6}Si_{0.4}$ . It was undoped film with calculated thickness of about 88 nm, but since Mg layer was a last layer during the annealing part of the Mg atoms can desorb and real thickness of formed films must be smaller than calculated one. The morphology of film is presented on Fig. 1. The top layer of film consists from non-oriented grains with sizes 40-80 nm, which have a small density of pinholes and they are not coalesced. The root mean square roughness is about 1.9 nm.

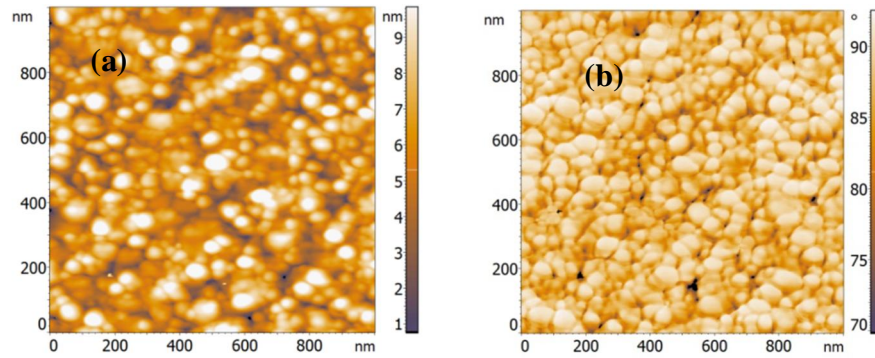


Figure 1. AFM images of  $\text{Mg}_2\text{Sn}_{0.6}\text{Si}_{0.4}$  film grown on Si(111) substrates without additional doping during Si-Sn-Mg three-layer formation procedure: (a) is amplitude contrast; (b) is phase contrast.

The next sample has calculated composition  $\text{Mg}_2\text{Sn}_{0.4}\text{Si}_{0.6}$  and thickness of about 63 nm. A significant difference was found in the morphology of this film (Fig. 2). Preferred orientation or texture was found in a film with this composition (Fig. 2 a). Grains have coalesced in one direction. They had a length of few hundred nanometers and width of about 50-100 nm only. The presence of texture nevertheless has not led to the crystallization of formed grains (Fig. 2 b). The root mean square roughness increases in nearly two times (3.7 nm) as compared with  $\text{Mg}_2\text{Sn}_{0.6}\text{Si}_{0.4}$  (Fig. 1).

The third sample had calculated composition  $\text{Mg}_2\text{Sn}_{0.4}\text{Si}_{0.6}$  and thickness of about 96 nm. Unlike the other two samples it was doped during growth by aluminum (Al) atoms. The grown film consists from grain with near equal sizes 60-80 nm, has some density of pinholes and root mean square roughness of about 2.4 nm (Fig. 3 a). Phase contrast image

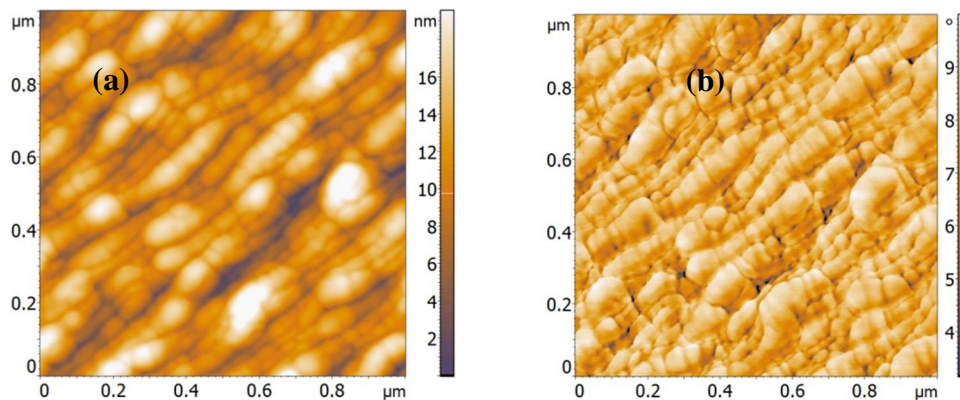


Figure 2. AFM images of  $\text{Mg}_2\text{Sn}_{0.4}\text{Si}_{0.6}$  film grown on Si(111) substrates (sample V482) without additional doping during Si-Sn-Mg three-layer formation procedure: (a) is amplitude contrast; (b) is phase contrast.

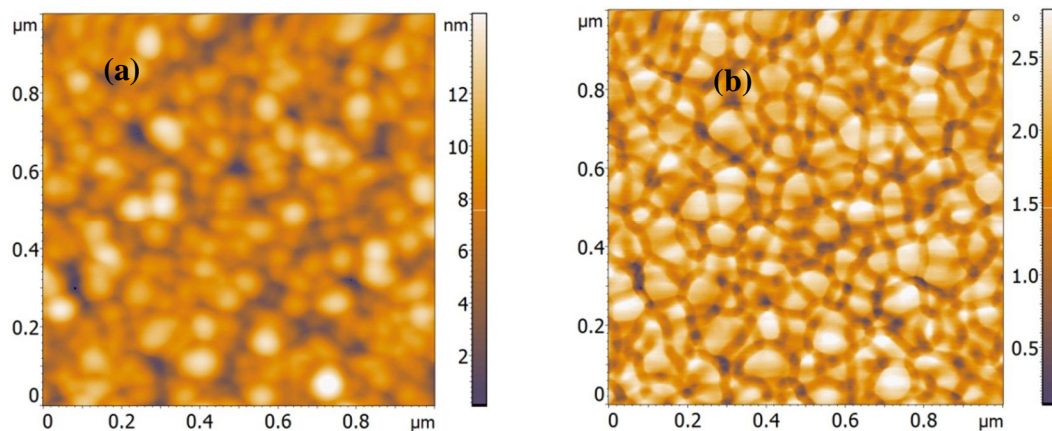


Figure 3. AFM images of  $\text{Mg}_2\text{Sn}_{0.4}\text{Si}_{0.6}$  film grown on Si(111) substrates with Al doping during Si-Sn-Mg three-layer formation procedure: (a) is amplitude contrast; (b) is phase contrast.

showed an appearance of some grain's facets and clearly visible darker borders between bright grains (Fig. 3 b), suggesting segregation of impurities between grains in the film due to the weak solubility of Al atoms in Mgstannide and Mg silicide at temperature  $150^\circ\text{C}$ .

Additional information about one of the sample ( $\text{Mg}_2\text{Sn}_{0.4}\text{Si}_{0.6}$ , sample V482) was obtained from TEM, and EFTEM data (Fig. 4). Figure 4(a) shows that the real thickness of grown Mg stannide-silicide film changes from 48 to 55 nm, which is close to calculated thickness (63 nm) from deposition rates and times for all elements. The interface between film and Si substrate is a nonsmooth. But a top part of the film is smoother that coincides with AFM data (Fig. 2). The distribution of elements on the cross-section is seen on Fig. 4(b,c,d), where elementary maps are presented. It is very heterogeneous, showing the non-uniform composition of the film thickness. The maximal Si concentration is seen in the middle of the film's thickness (Fig. 4 b). Mg concentration has two peaks: one is on the top of the film and another one is

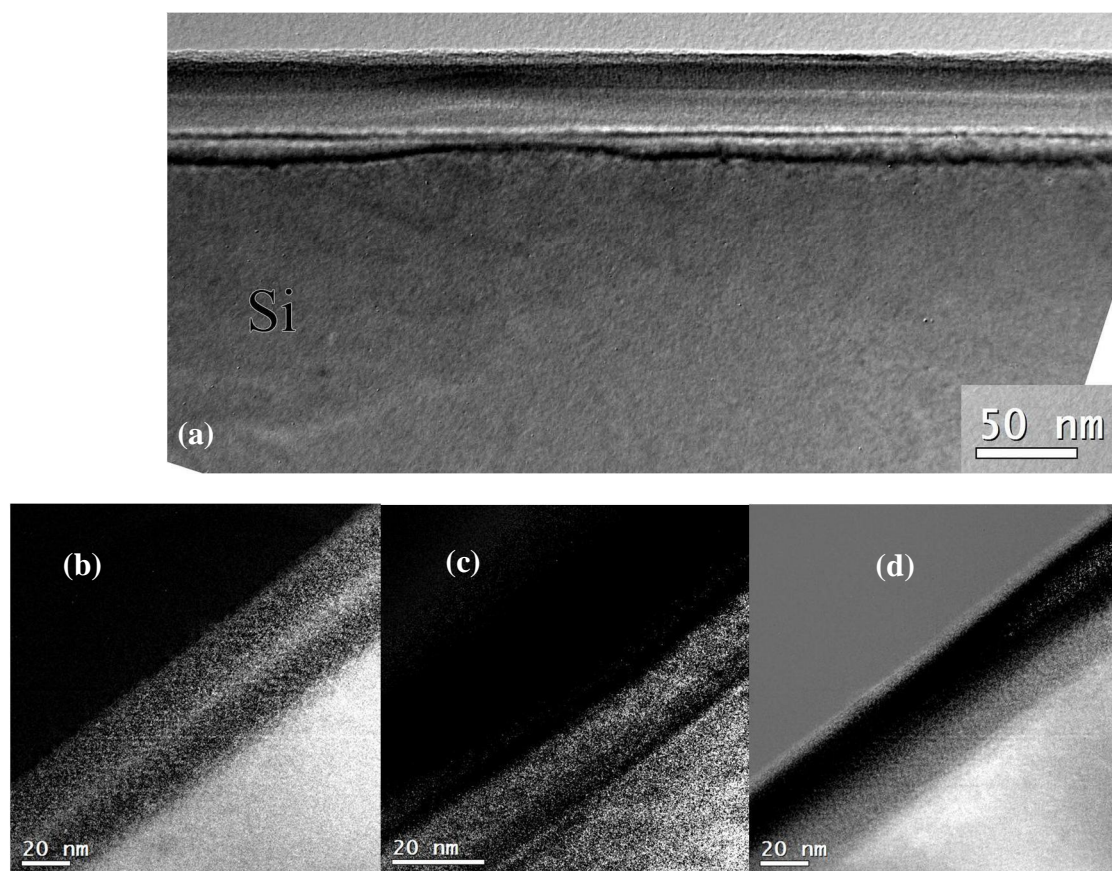


Figure 4. Cross-section TEM pattern of  $\text{Mg}_2\text{Sn}_{0.4}\text{Si}_{0.6}$  (V482) sample (a) and elementary maps in this sample: (b) Si map, (c) Sn map (d) Mg map.

on the interface with Si substrate (Fig. 4 d). The Sn map shows (Fig. 4 c) the main contribution of Sn atoms in the central part of the grown film. Near the silicon-film interface Sn concentration decreases, but non-uniformly along the interface. So, a layer-by-layer deposition of Si, Sn and Mg layers and single annealing at 150 °C do not contribute to uniform mixing of deposited layers and the formation of a homogeneous ternary alloy. Due to the heterogeneity of composition through the film thickness, one can expect the emergence of  $\text{Mg}_2\text{Si}$  and  $\text{Mg}_2\text{Sn}$  phases, as well as  $\text{Mg}_2\text{Si}_x\text{Sn}_{1-x}$  ternary alloy at different locations near the interface of the film with silicon.

The HR XTEM image of the sample V482 and its fast Fourier transformation (FFT) (Fig. 5) have proved the alternating composition and structure of layers along the interface of grown film with silicon. On the picture one can see that on the Si substrate – film interface from the film side an ordered layer was formed. Atomic planes in this layer are

Table 1. Interplanar distances calculated by FFT images.

	spot type	d(exp),nm	d(theor),nm	planes	Intensity,%
1-1'	point	0,1629	0,1637	fcc-Si(311)	
2-2'	point+line	0,3750	0,3800	hex- $\text{Mg}_2\text{Sn}$ (030)[1]	100
3-3'	point	0,1936	0,1919	fcc-Si(111)	
4-4'	circle	0,3164	0,3176	cub- $\text{Mg}_2\text{Si}$ (200)[2]	12
5-5'	point+line	0,3122	0,3135	fcc-Si(111)	
6-6'	circle	0,3716	0,3800	hex- $\text{Mg}_2\text{Sn}$ (300)[1]	100
7-7'	circle	0,2259	0,2246	cub- $\text{Mg}_2\text{Si}$ (220)[2]	100
8-8'	circle	0,3726	0,3800	hex- $\text{Mg}_2\text{Sn}$ (300)[1]	100



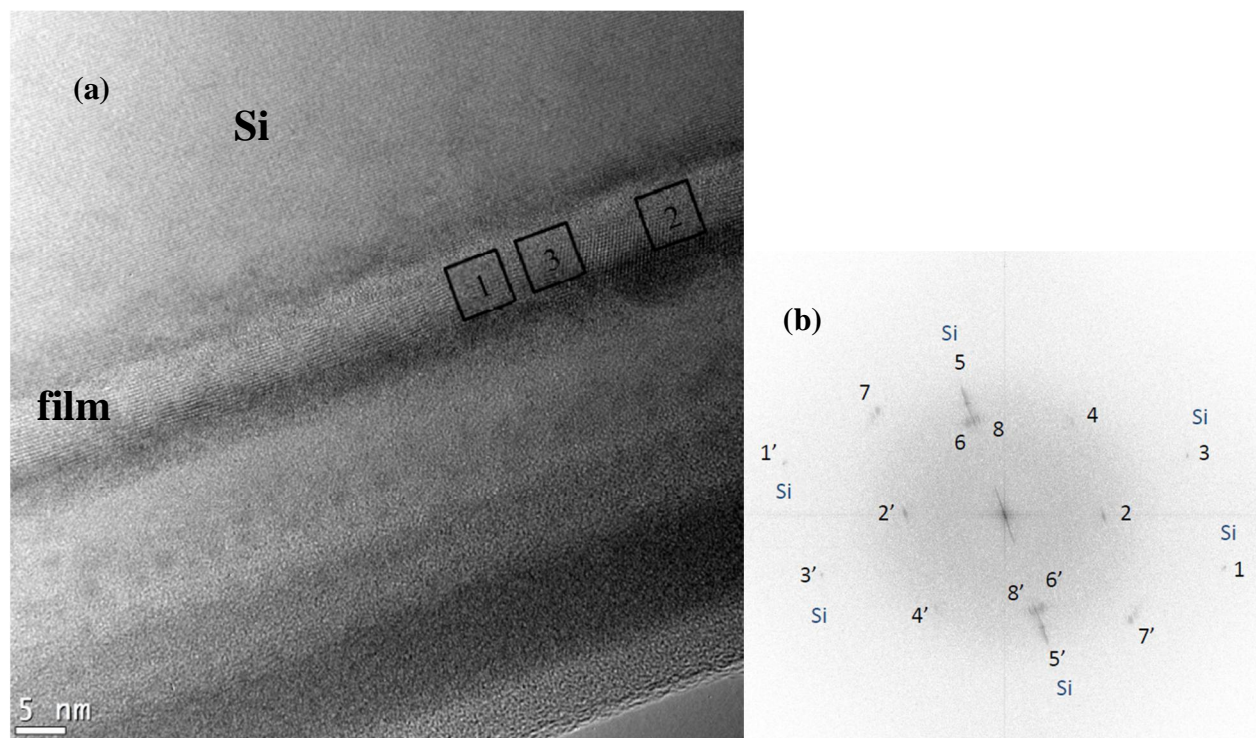


Figure 5.(a) Cross-section HR TEM pattern of  $\text{Mg}_2\text{Sn}_{0.4}\text{Si}_{0.6}$  film on the Si(111) substrate (sample V482). (b) Fast Fourier transformation (FFT) image of HR TEM pattern presented in (a). Reflexes of periodic structures are marked by numbers (1-8) and (1'-8'). Reflexes from the silicon substrate planes are marked with the Si. The framework of the marked area phase: (1) cub- $\text{Mg}_2\text{Si}$ +hex- $\text{Mg}_2\text{Sn}$ , (2) a single-domain hex- $\text{Mg}_2\text{Sn}$  and (3) a dual-domain hex- $\text{Mg}_2\text{Sn}$ .

parallel to atomic planes in the substrate. This indicates an epitaxial growth of ordered layer on a substrate. In some places of ordered layers the fields with another atomic planes and distance between them were observed. This indicates the formation of regions with other ordered structure in the epitaxial layer.

To determine interplanar distances in all ordered fields in Figure 5(a) the FFT analysis the entire image was performed. FFT image is presented in Figure 5(b). Six point reflexes (designated "Si") from well-structured periodic structure are in the picture. This structure is found in the upper left corner of Fig. 5(a) and corresponds to the monocrystalline silicon. From the symmetry of the arrangement of reflexes, it was suggested that the HR TEM image was obtained for the direction of the zone's axis [112]. In this case there are (220) and (311) reflexes from the Si(111) planes. Interplanar distances calculated from FFT image (Fig. 5(b)) confirmed these assumptions (see Table 1). Other reflexes are more blurred, indicating the variations of interplanar distances of some periodic structures that they describe. These periodic structures are located in the grown film.

Based on direct measurements (Fig. 5 a), the epitaxial film thickness of periodic structure grown on Si (111) substrate is small, so to analyse the periodic structures local FFT was used. But the most part of the film is an amorphous state, since has not any reflexes in FFT images (not shown). To analyse ordered part of the film, FFT images were taken from the selected square areas with size of 128 x 128 pixels. Research conducted at the film/Si substrate interface and in selected areas of epitaxial film.

It was found that near the interface there are reflexes from Si substrate and reflexes from the film. Reflexes from the film and from planes of Si (111) stretch. This behaviour of reflexes may occur if the small period change of periodic structure in the studied area and (or) disorientation of parallel planes. Apparently, near the film-substrate interface the crystalline structures of silicon and epitaxial film are deformed. Reflexes from the Si(111) planes are pulled in the direction of the line that runs through the central reflex. This means that at the silicon lattice deformation the interplanar distance in Si (111) plane, but disorientation (turning on small angle) of Si (111) planes does not occur. Reflexes from the film being pulled through the circle's arc with centre at the central reflex. This indicates the disorientation of parallel planes of the film substance.

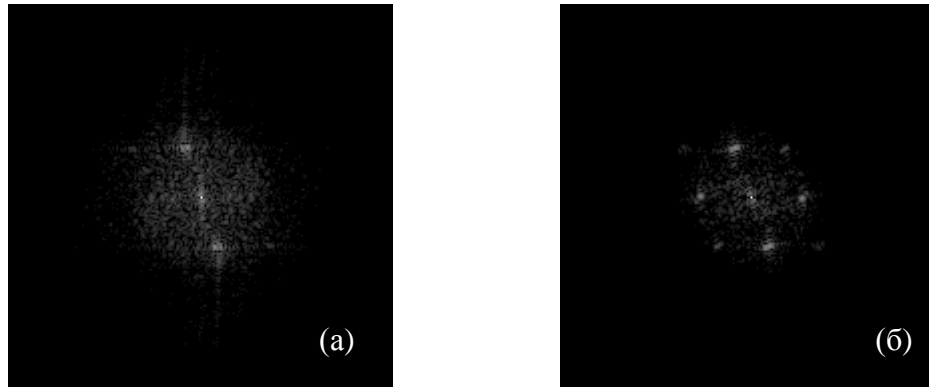


Figure 6. FFT images from arias 2 (a) and 3 (b) of the first group of periodic structures from Fig. 5(a). Interplanar distances, defined for structures, were similar to those obtained from Figure 5(b) for 6-6', 8-8' and 2-2' reflexes.

In the film there are areas with different periodic structure (see Figure 5 a). They can be divided into 2 groups. The first group includes structures with FFT images, shown in Figure 6. This periodic structure is characteristic for the whole epitaxial film, which has grown on Si (111) substrate. Interplanar distances, certain of the FFT images are appeared close to the distances between (300) and (030) planes of hexagonal magnesium stannide ( $\text{Mg}_2\text{Sn}$ )<sup>11</sup>. It can serve as proof of hexagonal  $\text{Mg}_2\text{Sn}$  film formation on Si(111) substrate. Epitaxial film of hexagonal  $\text{Mg}_2\text{Sn}$  grows not homogeneous: the formation areas of the single-domain (region 2 in Fig. 5a) and two-domain (area 3 on Fig. 5a) periodic structure are observed. The FFT picture from these areas there are, respectively, 2 (Fig. 6 a) and 4 (Fig. 6 b) bright reflexes. Elongated hexagonal reflexes of  $\text{Mg}_2\text{Sn}$  means that interplanar distance in the film of this  $\text{Mg}$ stannide is changed. In the layers close to the film-Si substrate interface with interplanar distance of hexagonal  $\text{Mg}_2\text{Sn}$ (300) (hex- $\text{Mg}_2\text{Sn}$ (300)) close to the value for planes of face centred cubic Si(111) (fcc-Si (111)) (see Fig. 7). Because the value of the interplanar distance of fcc-Si (111) (0.3135 nm) is less than the value for hex- $\text{Mg}_2\text{Sn}$ (300) in bulk material (0.38 nm) at 17.5%, then the hex- $\text{Mg}_2\text{Sn}$  film compressed in the border region to 17.5% in the direction perpendicular to the interface.

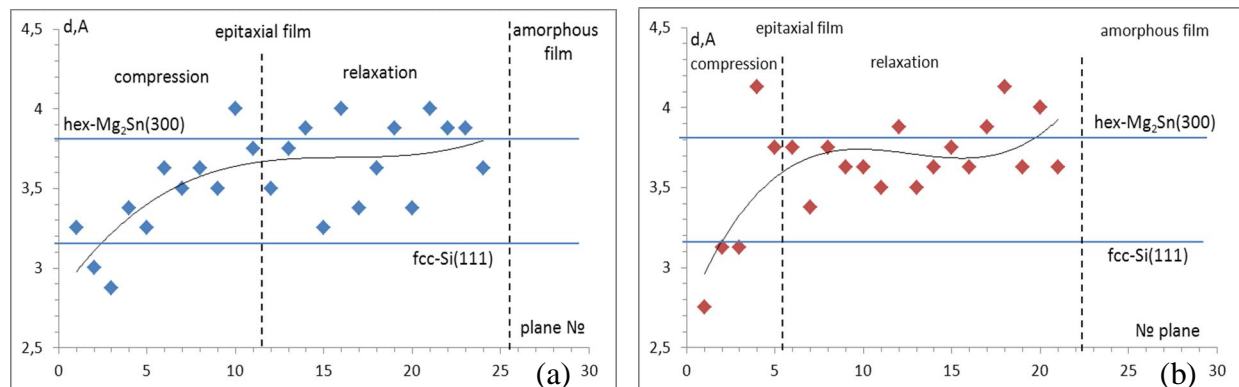


Figure 7. Interplanar distance ( $d$ ) in the hexagonal  $\text{Mg}_2\text{Sn}$  for the (300) plane, which number is calculated from the film – Si substrate interface: (a) for the areas with number 2 on Fig. 5(a); (b) for the areas with number 3 on Fig. 5(a).

While increasing numbers of hex- $\text{Mg}_2\text{Sn}$ (300) plane the interplanar(300) distance increases and at some number plane it reaches a value of 0.37 nm closer to interplanar distance for hex- $\text{Mg}_2\text{Sn}$  (300) in bulk material (0.38 nm). A further increase in the numbers of the plane does not change the interplanar distance for hex- $\text{Mg}_2\text{Sn}$ (300). This means that the compression caused by the mismatch of lattice constants for hex- $\text{Mg}_2\text{Sn}$ (300) and fcc-Si(111) were completely eliminated and the relaxation of hexagonal  $\text{Mg}$  stannide was came. The number of the plane, from which comes the relaxation of hex- $\text{Mg}_2\text{Sn}$ (300), depends on the type of the forming phase. For single-domain phase relaxation comes with 11 planes, whereas for two-domain -with 5 planes. Early onset of relaxation in two-domain phase was caused by stronger bonds between adjacent atoms in this phase than in single-domain phase.

The  $\text{Mg}_2\text{Sn}$  film epitaxially grows from the substrate, but upon reaching 23-25 layers begins to form an amorphous phase, and  $\text{Mg}_2\text{Sn}$  epitaxy stops. Because the film was formed by solid phase epitaxy, the complete cessation of epitaxial growth

can be caused by insufficient material (for example, atoms of Mg) at the front of a growing epitaxial film. The excess Sn atoms cannot react neither with atoms of Mg (because not enough atoms of Mg), nor with the atoms Sn (because the temperature of annealing temperature lower film crystallization of Sn). They form a thick amorphous layer, which prevents the diffusion of atoms of Mg in an area where there are not enough of them.

In addition to the reflexes of the hex-Mg<sub>2</sub>Sn on Fig. 6(b) there are reflexes of other periodic structure, which belongs to the second group. They are always seen together with hex-Mg<sub>2</sub>Sn reflexes of (see Fig. 6) even in the area where the phase from the second group occupies a larger area (area 1 on Fig. 5(a)) because hex-Mg<sub>2</sub>Sn phase forms the near continuous epitaxial film on the Si (111). Periodic structure from the second group occurs in the form of separate unrelated small areas vertically penetrating a film from the film-Si substrate interface to a layer of amorphous phase in the film. Interplanar distances, determined from FFT images appeared close to the distances between (200) and (220) planes of the cubic magnesium silicide (cub-Mg<sub>2</sub>Si)<sup>12</sup>. It can serve as proof of the formation of cub-Mg<sub>2</sub>Si islands on hex-Mg<sub>2</sub>Sn epitaxial film grown on Si(111) substrate.

Taking into account that islands are not linked, because the continuous cub-Mg<sub>2</sub>Si film is not formed, come to the conclusion that the cub-Mg<sub>2</sub>Si islands are epitaxially grown. However, the orienting role of the Si(111) substrate probably is not great, since the contact area of the island with the cub-Mg<sub>2</sub>Si and Si (111) substrate is small. It is possible that the hex-Mg<sub>2</sub>Sn film directs a growth of cub-Mg<sub>2</sub>Si island, because the contact area of the cub-Mg<sub>2</sub>Si island with hex-Mg<sub>2</sub>Sn film is great.

Determine the epitaxial relationships for hex-Mg<sub>2</sub>Sn film and Si (111) substrate. Figure 5(b) shows that the reflexes 6-6' and 8-8' (hex-Mg<sub>2</sub>Sn(300)) lie on the directions close to the 5-5' one (fcc-Si (111)). This means that the hex-Mg<sub>2</sub>Sn (300) plane is parallel to the fcc-Si(111) plane with small disorientation of  $\pm 2.9^\circ$ . Large mismatch of hex-Mg<sub>2</sub>Sn(300) and fcc-Si(111) lattices causes a large hex-Mg<sub>2</sub>Sn lattice compression in (300) plane (on -17.5%). Epitaxial growth in such conditions was possible if the parallel plane (the plane of the Si (111)) hex-Mg<sub>2</sub>Sn and fcc-Si are good matched. On the Si(111) surface the most suitable for matching with Mg<sub>2</sub>Sn(300) plane are distances between the nearest silicon atoms in directions fcc-Si [112] (0.665 nm) and fcc-Si[110] (0.3839 nm). The distances between adjacent Si atoms in these areas are close to the distances between atoms, respectively, in the direction hex-Mg<sub>2</sub>Sn[001] direction (0.699 nm, -5.1%) and hex-Mg<sub>2</sub>Sn[030] direction (0.38 nm, +1.0%). Mentioned directions are orthogonal among themselves. Considering the above, one can write the epitaxial relationship: hex-Mg<sub>2</sub>Sn [001]/fcc-Si[112] and hex-Mg<sub>2</sub>Sn[030]/fcc-Si[110].

Cross-sectional structure HR TEM studies have shown that epitaxial growth with annealing temperature 150°C in Mg stannide-silicide films is determined by raw composition on the interface, as well as protection from mixing with monocrystalline silicon. At the deposition of Sn on atomically clean monocrystalline silicon substrate the non-oriented island growth mode of cubic and hexagonal Mg<sub>2</sub>Sn was previously observed in amorphous matrix [new]. So, the previously deposited amorphous layer of Si defends from Si-Mg interaction and promotes chemical reaction between Sn and Mg atoms and epitaxial growth of hex-Mg<sub>2</sub>Sn. Part of the Mg atoms are chemically reacted with amorphous silicon and formed cubic Mg<sub>2</sub>Si islands inside epitaxial Mg<sub>2</sub>Sn film. Because orienting substrate influence is not very significant an epitaxial growth was shouted after 22-25 monolayer of Mg<sub>2</sub>Sn and next the growth of amorphous phases of variable composition was seen. The composition of the amorphous phase is difficult to determine the methods available, so consider the optical and electrical properties of grown magnesium stannide-silicide films.

Transmittance and reflectance spectra of Mg<sub>2</sub>Sn<sub>x</sub>Si<sub>1-x</sub> films grown by multilayer depositions of a-Si – Sn – Mg three-layers, with different Sn/Si relation, with and without doping by Al atoms are presented on Fig. 8 (a,b). Two type of compositions were realized: Mg<sub>2</sub>Sn<sub>0.6</sub>Si<sub>0.4</sub> and Mg<sub>2</sub>Sn<sub>0.4</sub>Si<sub>0.6</sub>. All grown Mg<sub>2</sub>Sn<sub>x</sub>Si<sub>1-x</sub> films have a decreasing absorbance at the energy decrease from 1.0 eV to 0.1 eV (Fig. 8 a). The decline of transmittance dependences in this energy range is maximal for Mg stannide-silicide with proposed Mg<sub>2</sub>Sn<sub>0.6</sub>Si<sub>0.4</sub> composition that corresponds to maximal fundamental band gap. Calculations of optical functions from transmittance and reflectance spectra of film-substrate system in the transparency region, including absorption coefficient, as well as from Kramers-Kronig integral relations have shown that fundamental shift in thin films of magnesium stannide-silicide cannot be determined due to the small density of states at the fundamental transition (apparently, indirect junction) and, accordingly, due to weak absorption. At this the direct interband transitions at 0.75 eV and 1.2 eV for film with Mg<sub>2</sub>Sn<sub>0.4</sub>Si<sub>0.6</sub> composition reliably enough have been recorded. For films with Mg<sub>2</sub>Sn<sub>0.6</sub>Si<sub>0.4</sub> and Al-Mg<sub>2</sub>Sn<sub>0.4</sub>Si<sub>0.6</sub> compositions several distinct values of the first direct interband transitions: 0.72 eV and 0.66 eV, respectively, were observed, but the second direct interband transition was nearly conserved at 1.2 eV.



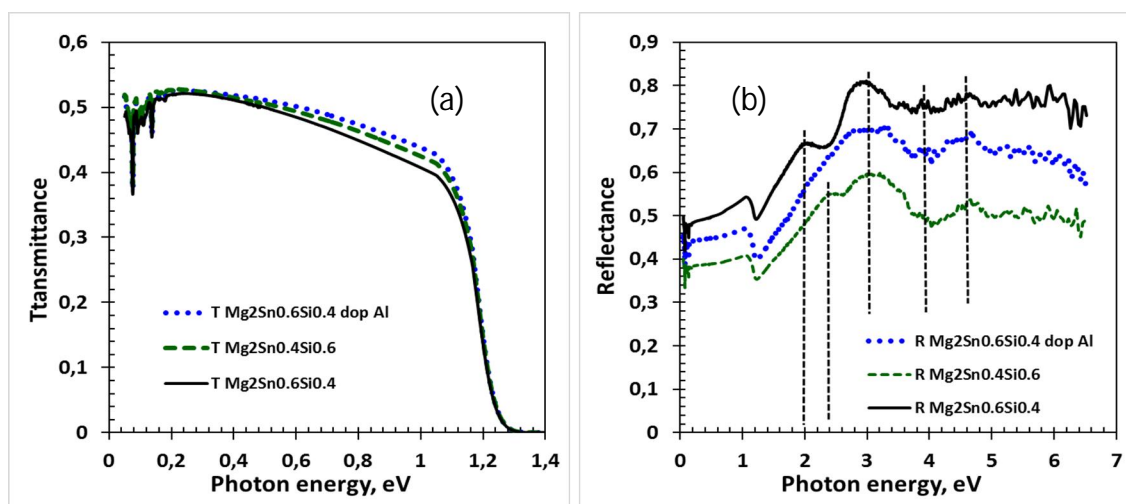


Figure 8. Reflectance (a) and transmittance (b) spectra of non-doped  $\text{Mg}_2\text{Sn}_{1-x}\text{Si}_x$  and Al doped  $\text{Mg}_2\text{Sn}_{1-x}\text{Si}_x$  films on Si(111) substrate.

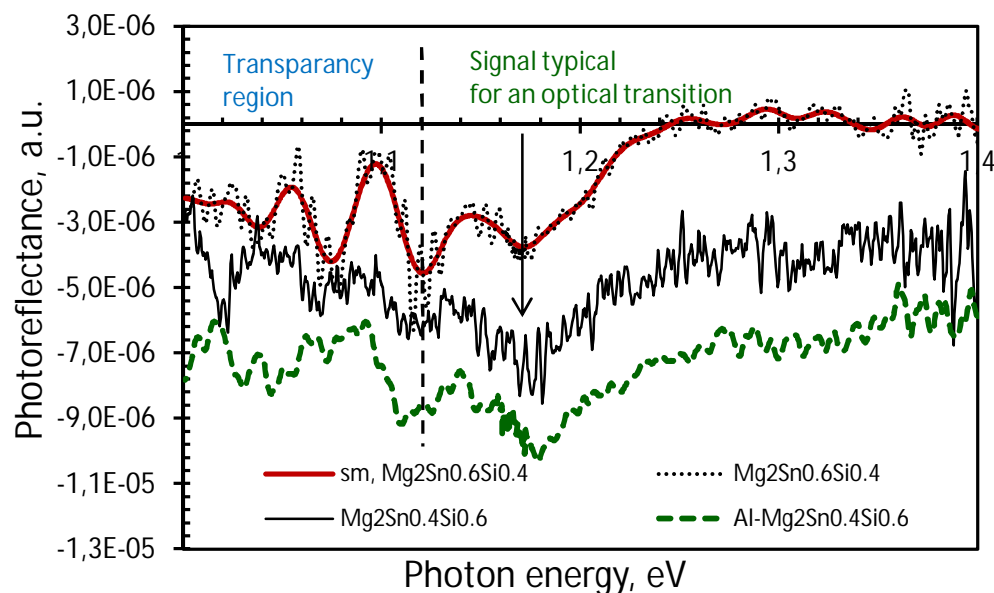


Figure 9. Photoreflectance (PR) spectra at room temperature together with its fitting by Fourier decomposition method with 20 points on a curve (red solid line ("sm") for  $\text{Mg}_2\text{Sn}_{0.6}\text{Si}_{0.4}$  sample) for Mg stannide-silicide films on silicon substrate:  $\text{Mg}_2\text{Sn}_{0.4}\text{Si}_{0.6}$  (black solid line),  $\text{Mg}_2\text{Sn}_{0.6}\text{Si}_{0.4}$  (black dots) and Al- $\text{Mg}_2\text{Sn}_{0.4}\text{Si}_{0.6}$  (green dashed line). The transparency region of silicon substrate begins from photon energy lower 1.12 eV. Two PR spectra are shifted on the "y" axis by the amount of  $5 \times 10^{-6}$  a.u. on "y" axis as compared with real spectra.

It was observed that in reflectance spectra of non-doped and Al doped  $\text{Mg}_2\text{Sn}_x\text{Si}_{1-x}$  films (Fig. 8 b) the maxima are observed at photon energies: 2.0-2.40, 2.80-3.05, 3.76-3.8 and 4.4 – 4.5 eV. These peaks are not the same as for  $\text{Mg}_2\text{Sn}$  monocrystal<sup>13</sup>: 2.12, 2.73, 2.96, 3.41 and 3.83 eV that confirms the declination from  $\text{Mg}_2\text{Sn}$  and  $\text{Mg}_2\text{Si}$  stoichiometry's and formation of alloy composition.

A strong direct interband transition with great oscillator force was confirmed photoreflectance spectroscopy data (Fig. 9), registered at room temperature for three films with two compositions:  $\text{Mg}_2\text{Sn}_{0.4}\text{Si}_{0.6}$   $\text{Mg}_2\text{Sn}_{0.6}\text{Si}_{0.4}$ . The position of the main interband transition in films of both compositions grown with and without Al doping begins with equal energy 1.17 eV that coincides with the computations of the energies of interband transitions (1.2 eV) from transmission and reflection

spectra. At lower photon energies a transparency region of silicon begins that not allows to estimate the contribution of direct interband transitions with energy less than 1.0 eV.

To determine the area, in which a dispersion is absence ( $n = n_o = \text{const}$ ), and one can speak about the existence of a fundamental transition in thin film with small absorption, you must build the dependence of  $1/(n^2-1)$  by  $\lambda^{-2}$  (where  $\lambda$  is the wavelength of the incident radiation). Extrapolation of the linear part of the  $1/(n^2-1)$  dependence to  $\lambda^{-2} = 0$ <sup>14</sup> allows to calculate the amount of undispersed refractive index ( $n_o$ ). This dependence for film with  $\text{Mg}_2\text{Sn}_{0.4}\text{Si}_{0.6}$  composition is presented on Fig. 10. One can see that the linear plot of this dependence ends at  $1/\lambda^2$  value equal to 0.02, which corresponds to the energy of the photons about 0.18 eV. Therefore, the fundamental transition in the film with  $\text{Mg}_2\text{Sn}_{0.4}\text{Si}_{0.6}$  composition exists at larger photon energy in the range from 0.2 eV to 0.3 eV. This correlates with the data obtained from the absorption coefficient spectrum. The value of non-dispersed refractive index calculated at the value  $1/\lambda^2 = 0$  equals to  $n_o = 3.59 \pm 0.01$ . One can calculate through the received amount a low-frequency (non-dispersed) dielectric constant of the grown film:  $\epsilon_o = n_o^2 = 12.89$ .

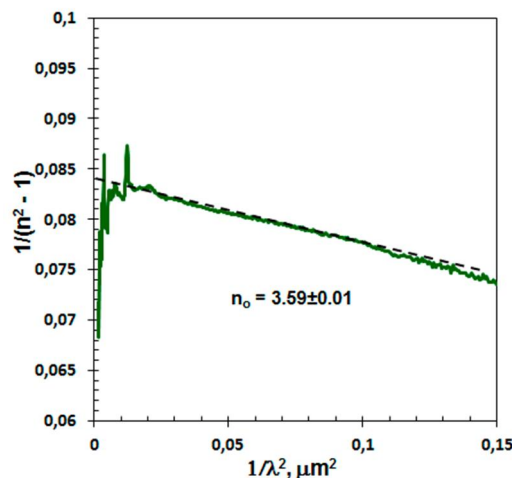


Figure 10. Dependence  $(n^2-1)^{-1}$  versus  $1/\lambda^2$  for non-doped film with  $\text{Mg}_2\text{Sn}_{0.4}\text{Si}_{0.6}$  composition. The dashed line shows the approximation to the value of  $1/\lambda^2 = 0$ .

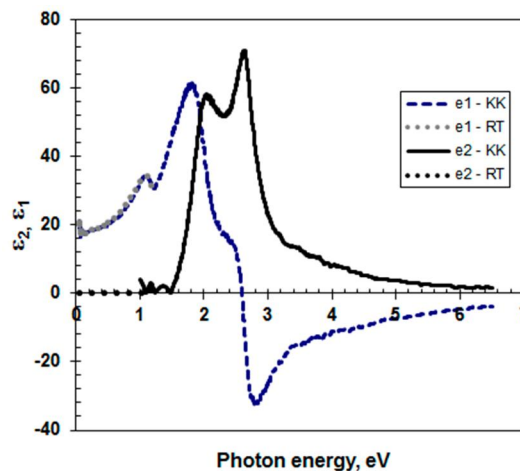


Figure 11. Real ( $\epsilon_1$ ) and imaginary ( $\epsilon_2$ ) parts of dielectric function for non-doped film with  $\text{Mg}_2\text{Sn}_{0.4}\text{Si}_{0.6}$  composition, calculated from Kramers-Kronig (KK) integral relations and two-layer model (RT) of the film-substrate system<sup>15</sup>.

For the calculation of the refractive index and dielectric functions in the area of basic interband transitions the

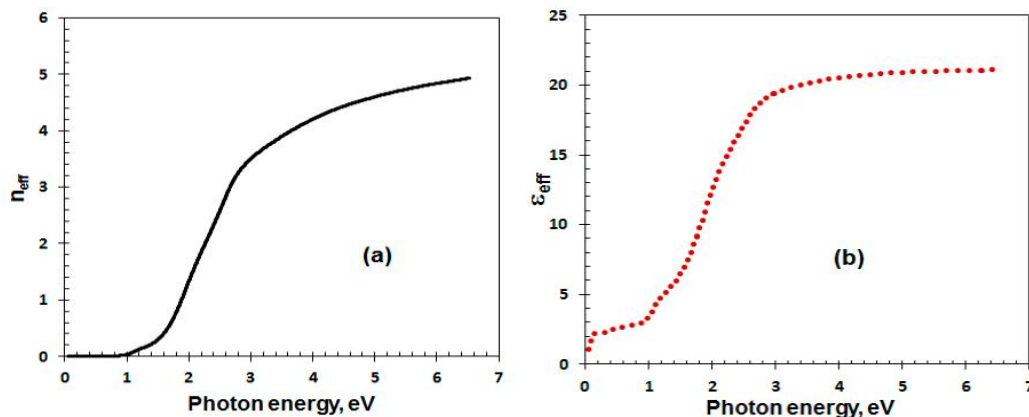


Figure 12. Photon energy dependences of electron effective number on the unit cell ( $n_{\text{eff}}$ ) and effective dielectric constants ( $\epsilon_{\text{eff}}$ ) for the film with  $\text{Mg}_2\text{Sn}_{0.4}\text{Si}_{0.6}$  composition.

integral Kramers-Kronig relations in the energy range from 1.0 eV to 6.5 eV were used. To do this, use the reflectance spectrum data (Fig. 8 b) and use datum point calculations ( $n_r$  and  $k_r$ ) in the beginning of the film strong absorption at energy of about 1.17 eV, calculated from double-layer model (model RT). Figure 11 shows the functions of real ( $\epsilon_1$ ) and imaginary ( $\epsilon_2$ ) parts of the dielectric function of the film with  $\text{Mg}_2\text{Sn}_{0.4}\text{Si}_{0.6}$  composition, calculated from Kramers-Kronig integral relations and RT model<sup>15</sup>. It is seen that in the field of photon energies up to 1.2 eV they are fully consistent in amplitude and  $\epsilon_1$  character and begin to match from energies of about 1 eV for  $\epsilon_2$ . Basic transitions in accordance with the function of the imaginary part of the dielectric function is observed at 2.0 eV and 2.6 eV, which are described by  $M_0$  and  $M_1$  type's critical points. Weaker interband transition is observed at energies around 3.5 eV with a large half-peak width that is characterized by transitions in several points of the Brillouin zone. This is consistent with the theoretical calculations of dielectric function for three-dimensional  $\text{Mg}_2\text{Sn}$  and  $\text{Mg}_2\text{Si}$ <sup>16</sup>. The obtained values of critical points lie between stoichiometric magnesium stannide and magnesium silicide, indicating the formation of a ternary alloy.

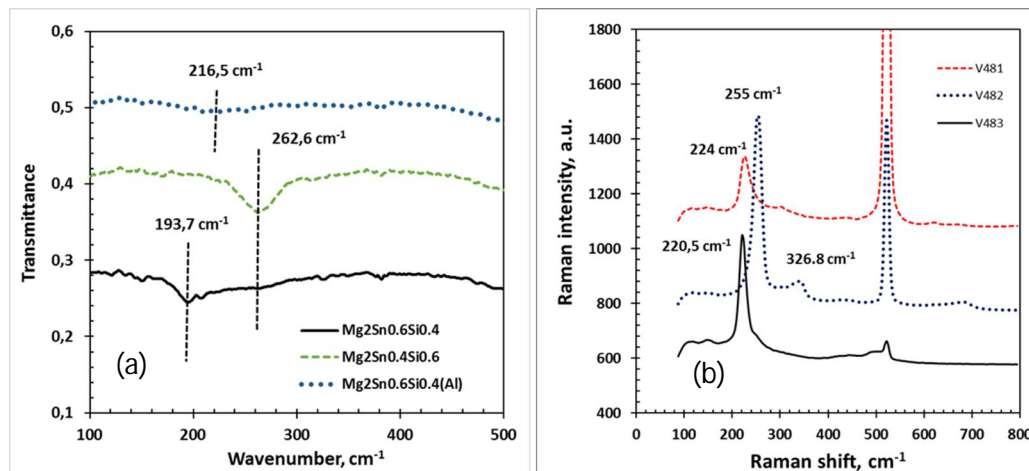


Figure 13. Far infrared (a) and Raman (b) spectra of un-doped and Al doped  $\text{Mg}_2\text{Sn}_{1-x}\text{Si}_x$  films.

Using optical sum rules<sup>17</sup>, as well as the real and imaginary part of the dielectric function the dependences of the electron effective number on the unit cell ( $n_{\text{eff}}$ ) and effective dielectric constants ( $\epsilon_{\text{eff}}$ ) versus the photon energy can be calculated. These dependences are presented in Fig. 12(a,b). Effective number of valence electrons in a unit cell (Fig. 12 a) is determined by the contributions of the various interband transitions. At these transitions with energies greater than 2 eV introduce the main contribution. Bearing in mind that in the magnesium stannide unit cell are 8 electrons<sup>16</sup>, then the interband transitions with energies up to 6.5 eV no more than 5 valence electrons accounted for. On the contrary, interband transitions with energies from 2 eV to 3 eV made the main contribution to the effective dielectric constant (Fig. 12 b).

Vibrational properties of all grown Mg stannide and Mg stannide-silicide films were studied by Fourier transmittance spectroscopy and Raman spectroscopy at room temperature. Transmittance spectra in far infra-red region (two bottom ones are artificially shifted on 0.1 and 0.2) for un-doped and doped  $\text{Mg}_2\text{Sn}_x\text{Si}_{1-x}$  films shown (Fig. 13 a) the formation of the one peak shifted from known position for  $\text{Mg}_2\text{Sn}$  bulk crystal<sup>18</sup> at  $189\text{ cm}^{-1}$ . The close value  $193.7\text{ cm}^{-1}$  has a film with estimated composition  $\text{Mg}_2\text{Sn}_{0.6}\text{Si}_{0.4}$ , which did not doped during growth process. But the  $\text{Mg}_2\text{Sn}_{0.6}\text{Si}_{0.4}$  film doped by Al atoms has the negligible intensity and very broad peak at  $216.5\text{ cm}^{-1}$ . Only one peak ( $220.5$  or  $224\text{ cm}^{-1}$ ) was also observed in Raman spectra (Fig. 13 b) of non-doped and Al doped films with estimated composition  $\text{Mg}_2\text{Sn}_{0.6}\text{Si}_{0.4}$ . This position is closed to Raman peak position for bulk  $\text{Mg}_2\text{Sn}$   $222.3\text{ cm}^{-1}$ <sup>19</sup>. The presence of only one peak as in FIR transmittance and Raman spectra allow to assume the formation of ternary compound with composition enriched by Sn.

The film with estimated composition  $\text{Mg}_2\text{Sn}_{0.4}\text{Si}_{0.6}$  has the FIR-peak with position at  $262.6\text{ cm}^{-1}$  (Fig. 13 a) closed to position for bulk  $\text{Mg}_2\text{Si}$  ( $267\text{ cm}^{-1}$ )<sup>20</sup>. This is confirmed by Raman spectrum, in which one can see single peak ( $255\text{ cm}^{-1}$ ) close to position in bulk  $\text{Mg}_2\text{Si}$  ( $258\text{ cm}^{-1}$ )<sup>20</sup>. Therefore, when the portion of Sn during layer-by-layer deposition was smaller than Si portion the real composition of Mg stannide-silicide is closed to  $\text{Mg}_2\text{Si}$ .

## 4. CONCLUSIONS

$\text{Mg}_2\text{Sn}_x\text{Si}_{1-x}$  un-doped and Al doped layers with two compositions were prepared by solid phase deposition of Si-Sn-Mg multilayers (8) on atomically clean Si(111)7x7 substrate and single annealing at  $150^\circ\text{C}$ . It was shown that grown films are nonhomogeneous on the thickness and composition ( $\text{Mg}_2\text{Sn}$ ,  $\text{Mg}_2\text{Si}$ ,  $\text{Mg}_2\text{Sn}_x\text{Si}_{1-x}$ ). Grown films consist from thin (5-7 nm) and compressed epitaxial layer of hex- $\text{Mg}_2\text{Sn}$  on the interface with Si substrate and thick 40-80 nm of amorphous Mg silicide, Mg stannide and ternary Mg stannide-silicide with variable compositions by data of transmittance electron microscopy. Using of fast Fourier transformation permit to determine an epitaxial relationship: hex- $\text{Mg}_2\text{Sn}$ (300)//Si(111), hex- $\text{Mg}_2\text{Sn}$ [001]||Si[-112] and hex- $\text{Mg}_2\text{Sn}$ [030]||Si[110] in the compressed epitaxial layer on the interface with Si substrate for three-component multilayer Si-Sn-Mg system. Optical properties of grown films were studied by optical spectroscopy and photoreflectance spectroscopy. Calculation of optical functions was done from Kramers-Kronig integral relations and from reflectance and transmittance spectra using two-layer model. The fundamental transitions in grown Mg stannide-silicide films could not be determined due to small thickness of films and small value of the absorption coefficient near the band gap edge. From calculated refraction index function the undispersed region (lower 0.18 eV) and value of the undispersed refraction index ( $n_0 = 3.59 \pm 0.01$ ) were determined. The main absorption in grown films starts from near 0.7-0.8 eV that corresponds to the first interband transition at 0.75-0.76 eV. The strongest interband transition was found at 1.2 eV from refraction and dielectric functions and confirmed by data of photoreflectance spectroscopy (1.17 eV) at room temperature. From the imaginary part of the dielectric function the electron effective number on the unit cell ( $n_{\text{eff}}$ ) and effective dielectric constants ( $\epsilon_{\text{eff}}$ ) versus the photon energy were calculated, using optical sum rules. It was determined that the main contribution in the function of effective number of valence electrons give interband transitions with energies higher than 2 eV and in this process participate more than 5 valence electrons. Additional growth experiments need to eliminate the heterogeneity of the film composition by reducing the thickness of the Si-Sn-Mg three-layer, increasing the number of three-layers and optimizing of the annealing time. As low band gap materials Mg stannide-silicide films need the electrical and thermoelectrical measurements and determination of their electrical and photoelectrical parameters.

## ACKNOWLEDGEMENTS

This work is partially supported by RFBR grant No 16-52-00074-Bel-a, by Belarusian Science Foundation for Fundamental Research (No. F16R-048) and by the Hungarian National Scientific Research Fund (OTKA) Grant No. K108869. Part of this work was supported by the Ministry of Education and Science of the RF (Grant Nos. NSh-6889.2016.2).



## REFERENCES

- [1] Fazquez, F., Forman, R.A., Cardona M., "Electroreflectance Measurements on  $\text{Mg}_2\text{Si}$ ,  $\text{Mg}_2\text{Ge}$ , and  $\text{Mg}_2\text{Sn}$ ," Phys. Rev. 176 905-908 (1968).
- [2] Zaitsev, V.K., Fedorov, M.I., Gurieva, E.A., Eremin, I.S., Konstantinov, P.P., Samunin, A.Yu., and Vedernikov, M. V., "Highly effective  $\text{Mg}_2\text{Si}_{1-x}\text{Sn}_x$  thermoelectrics," Phys. Rev. B, 74, 045207(1-8) (2006).
- [3] Chen, H. Y., Savvides N., "Microstructure and Thermoelectric Properties of n- and p-Type Doped  $\text{Mg}_2\text{Sn}$  Compounds Prepared by the Modified Bridgman Method," Journal of Elect. Mater., 38, 1056-1061 (2009).
- [4] Asaka, M., Iida, T., Nishio, K., Takanashi, Y., "Composition dependent thermoelectric properties of sintered  $\text{Mg}_2\text{Si}_{1-x}\text{Ge}_x$  ( $x = 0$  to 1) initiated from a melt-grown polycrystalline source," Thin Solid Films, 515, 8237-8241 (2007).
- [5] Ihou-Mouko, H., Mercier, C., Tobola, J., Pont, G., Scherrer, H., "Thermoelectric properties and electronic structure of p-type  $\text{Mg}_2\text{Si}$  and  $\text{Mg}_2\text{Si}_{0.6}\text{Ge}_{0.4}$  compounds doped with Ga," J. Alloy and Compounds, 509, 6503-6508 (2011).
- [6] Morrison, R.G., Fedin, R.D., G.C. Danielson, G.C., "Semiconducting Properties of  $\text{Mg}_2\text{Si}$  Single Crystals," Phys. Rev., 109, 1909-1915 (1958).
- [7] Morrison, R.G., Fedin, R.D., Danielson, G.C., "Semiconducting Properties of  $\text{Mg}_2\text{Ge}$  Single Crystals," Phys. Rev., 109, 1916-1920 (1958).
- [8] Tani, J., H. Kido, H., "Thermoelectric properties of Bi-doped  $\text{Mg}_2\text{Si}$  semiconductors," Physica B, 364, 218-224 (2005).
- [9] Tani, J., H. Kido, H., "Thermoelectric properties of Sb-doped  $\text{Mg}_2\text{Si}$  semiconductors," Intermetallics, **15**, 1202-1207 (2007).
- [10] Galkin, N.G., Galkin, K.N., Goroshko, D.L., Chervnev, I.M., Shevlyagin, A.V., Dózsa, L., Osváth, Z., Pécz, B., "Non-doped and doped Mg stannide films on Si(111) substrate: formation, optical and electrical properties," Jap. J. Appl. Phys., 54, 07C06(1-9), (2015).
- [11] Dyuzheva, T.I., Kabalkina, S.S., Vereshchagin, L.F., "Polymorphism of  $\text{Mg}_2\text{Sn}$  at high temperatures and pressures," Sov. Phys. Crystallogr. (Engl. Transl.) 17, 705-710 (1973).
- [12] Natl. Bur. Stand. (U.S.) Monogr. 25, 21, 86 (1984).
- [13] Vazquez, F., Forman, R.A., Cardona, M., "Electroreflectance Measurements on  $\text{Mg}_2\text{Si}$ ,  $\text{Mg}_2\text{Ge}$ , and  $\text{Mg}_2\text{Sn}$ ," Phys. Rev., 176, 905-908 (1968).
- [14] Palik, E.D., (Ed.), *Handbook of Optical Constants of Solids*, Academic Press, 1985.
- [15] Galkin, N.G., Maslov, A.M., Konchenko, A.V., "Optical and photospectral properties of  $\text{CrSi}_2$  A-type epitaxial films on Si(111)," Thin Solid Films, 311, 230-238 (1997).
- [16] Scooler, W.J., "Optical properties of  $\text{Mg}_2\text{Si}$ ,  $\text{Mg}_2\text{Ge}$  and  $\text{Mg}_2\text{Sn}$  from 0.6 to 11 eV at 77K," Physical Review, 178, 1353-1357 (1969).
- [17] Edward D. Palik (Ed.), *Handbook of Optical Constants of Solids*, Academic Press, 1985.
- [18] Geik, R., Hakel W.J., Perry, C.H., "Temperature Dependence of the Far-Infrared Reflectivity of Magnesium Stannide," Phys. Rev., 148, 824-827 (1966).
- [19] Whitten, W.B., Chung, P.L., Danielson, G.C., "Lattice dynamics of  $\text{Mg}_2\text{Ge}$ ," J. Phys. Chem. Solids., 26, 1753-1760 (1965).
- [20] McWilliams, D., Linch, D.W., "Infrared Reflectivities of Magnesium Silicide, Germanide, and Stannide," Phys. Rev., 130, 2248-2252 (1963).